ISSN 1064-2269, Journal of Communications Technology and Electronics, 2016, Vol. 61, No. 5, pp. 453–468. © Pleiades Publishing, Inc., 2016.
Original Russian Text © A.S. Godin, M.S. Matsayan, K.N. Klimov, 2016, published in Radiotekhnika i Elektronika, 2016, Vol. 61, No. 5, pp. 401–417.

ELECTRODYNAMICS AND WAVE PROPAGATION

Numerical Electrodynamic Analysis of the External Sestroretskii Cube

A. S. Godin, M. S. Matsayan, and K. N. Klimov

Lianozovo Electromechanical Plant Research and Production Corporation, Dmitrovskoe sh. 110, Moscow, 127411 Russia
e-mail: andrey.godin@gmail.com, const0@mail.ru

Received October 21, 2014

Abstract—The paper presents the results of numerical analysis of the frequency characteristics of the external Sestroretskii cube and the comparison of them with the frequency characteristics of the internal cube. It is shown that the external Sestroretskii cube has the properties of a frequency diplexer and a double waveguide triplexer and, at low frequencies, the absolute values of its transmission coefficients tend to those of the internal cube.

DOI: 10.1134/S1064226916050065

1. ANALYSIS OF THE EXTERNAL SESTRORETSKII CUBE

Consider a cube A with the dimensions of $1 \times 1 \times 1$ mm (Fig. 1). The cube A is filled with metal. To each face of the cube A, a rectangular parallelepiped also filled with metal is attached. The bases of the rectangular parallelepipeds coincide with the faces of the cube A and have the same height $h = 0.05$ mm. However, we are going to calculate the properties of the cube as $h \to 0$; therefore, after the numerical determination of the scattering matrix of the external Sestroretskii cube by means of the ANSYS HFSS v.15 code [1], we will move the reference input planes of the device [2] up to the contact with the cube A. The number of rectangular parallelepipeds is six, which equals the number of faces of the cube A. Select in Fig. 2 the faces of rectangular parallelepipeds adjacent to the cube A, and impose on them the zero boundary conditions for the tangential component of the electric field, E_τ, which corresponds to a metal wall. These faces will be considered the short-circuit (SC) walls [2–4].

In Fig. 3, select the faces of the same parallelepipeds but with the zero boundary condition for the tangential component of the magnetic field, H_τ, which corresponds to a magnetic wall. These faces will be considered the open-circuit (OC) walls [2–4].

On the remaining faces of the rectangular parallelepipeds connected to the cube A (Fig. 4), impose the boundary conditions of excitation and matching of plane waves [2–4], which correspond to the ports of the external Sestroretskii cube. In Fig. 4, all ports are also enumerated. The polarizations of the electric, $\vec{E}$, and magnetic, $\vec{H}$, fields and the directions of the Poynting vectors $\vec{S}$ [5–8] of the incident plane waves are shown in Fig. 5.

For the consideration of the external electrodynamic problem, place the suggested geometry with the above boundary conditions into an air cube B (Fig. 6), on the faces of which impose the radiation conditions [1]. The external air cube B has the dimensions of $5 \times 5 \times 5$ mm. The cube B is filled with vacuum.

Figure 7 shows the faces of the cube B, on which the radiation boundary conditions are imposed.

The metal-filled cube A together with the six metal-filled rectangular parallelepipeds connected to its faces, all being placed in an air cube B with the boundary conditions introduced above, will be called the external Sestroretskii cube.

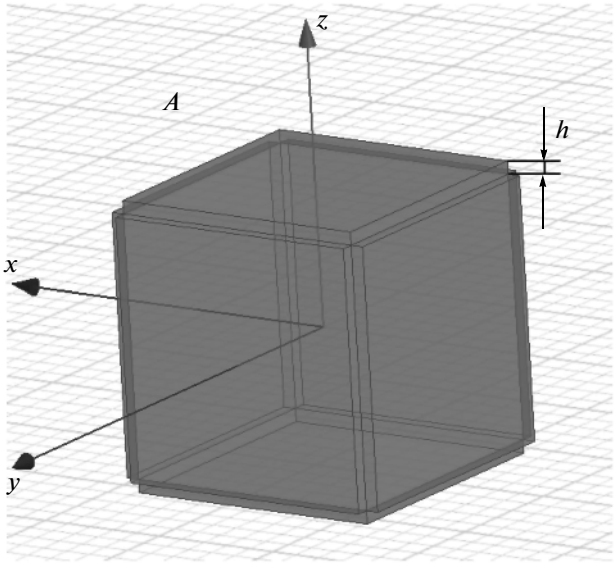

Fig. 1. Geometry of cube A and metal-filled rectangular parallelepipeds attached to its faces.

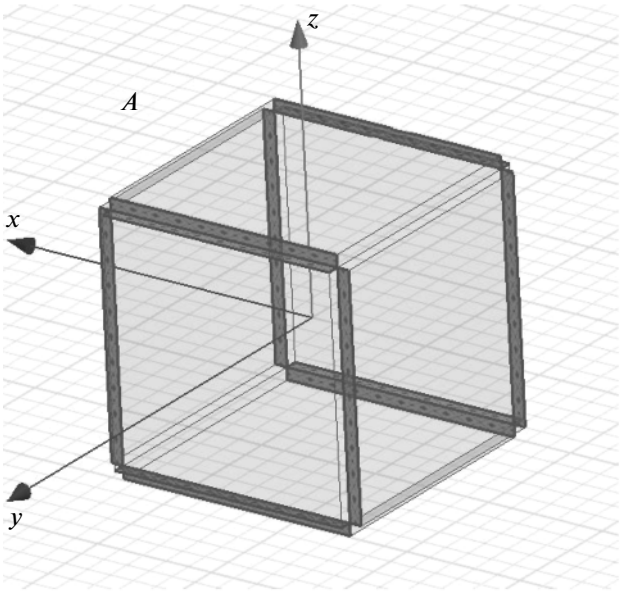

Fig. 2. Faces of rectangular parallelepipeds on which the SC condition is imposed.

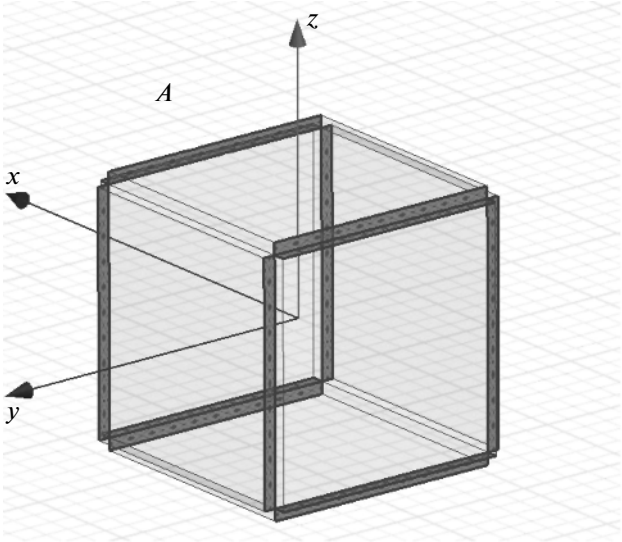

Fig. 3. Faces of rectangular parallelepipeds on which the OC condition is imposed.

The external Sestroretskii cube is symmetric and, therefore, its scattering matrix can be found from the scattering matrices of the halves of the cube under the in-phase and antiphase excitations [2, 9–13].

2. THE EXTERNAL SESTRORETSKII CUBE UNDER IN-PHASE EXCITATION

Consider the external Sestroretskii cube under the in-phase excitation of ports *1* and *2* (see Fig. 4). Under such an excitation, the problem of electromagnetic-wave scattering is equivalent to the problem with the geometry shown in Fig. 8, which is the upper half of the initial geometry on the lower face of which the OC condition is imposed [2, 9–13]. This geometry will be called the geometry of the external half of the Sestroretskii cube under an in-phase excitation (EHSCIE) and denoted by A^{++}.

Figure 9 shown the faces of an EHSCIE on which the OC boundary conditions are imposed, and Fig. 10 shows the faces of an EHSCIE with the SC boundary conditions. The numeration of the ports on which the boundary conditions of matching and excitation of electromagnetic waves are imposed is the same as in the initial geometry (see Fig. 4).

Figure 11 shows the faces on which the radiation boundary conditions are imposed for the EHSCIE A^{++}, and Fig. 12 shows the faces of the EHSCIE with the imposed conditions of excitation and matching of planes waves [2–4]. The polarizations of the electric and magnetic field and the directions of the Poynting vectors [5–8] of these plane waves are shown in Fig. 13.

The simulation of the problem of electromagnetic-wave scattering by the EHSCIE was performed by means of the ANSYS HFSS v.15 software package for 3D electromagnetic modeling [1].

3. RESULTS OF SIMULATION OF A HALF OF THE SESTRORETSKII CUBE UNDER IN-PHASE EXCITATION

The calculation will be performed in a frequency band of 1 to 300 GHz with a step of 1 GHz. The tolerance for the absolute values of the components of the scattering matrix was Delta S = 0.02. The total number of tetrahedra was 28034, and the size of the resulting matrix was 180548, which required 1.17 GB of RAM. The total computation time on a PC with an Intel Core i7 2.79 GHz processor and 12 GB RAM was 7 h 19 min 55 s.

Figure 14 presents the frequency characteristic of the SWR of the EHSCIE. Near the frequency of 1 GHz, the edge length of the EHSCIE is 1/300 of the wavelength. This is a quasi-static case. The SWR at the frequency of 1 GHz is 1.01. As the frequency increases to 64 GHz, the SWR increases to the maximum value of 2.23. Then the SWR decreases and, at the frequency of 150 GHz, which corresponds to the edge length of the EHSCIE at the half-wavelength, is 1.24. Then, at the frequency of 200 GHz, the SWR is 1.07, at the frequency of 250 GHz decreases to 1.06, and at the frequency of 300 Hz (the edge length of EHSCIE equals the wavelength) the SWR increases again and equals 1.07.

Figure 15 shows the frequency characteristic of the absolute value of the reflection coefficient S_{22} for port *2* of the EHSCIE, from which we see that at the frequency of 1 GHz, (1/300 of the wavelength) the output return loss is –43.5 dB. At the frequency of 64 GHz, the output return loss reaches –8.37 dB. Then, at the fre-

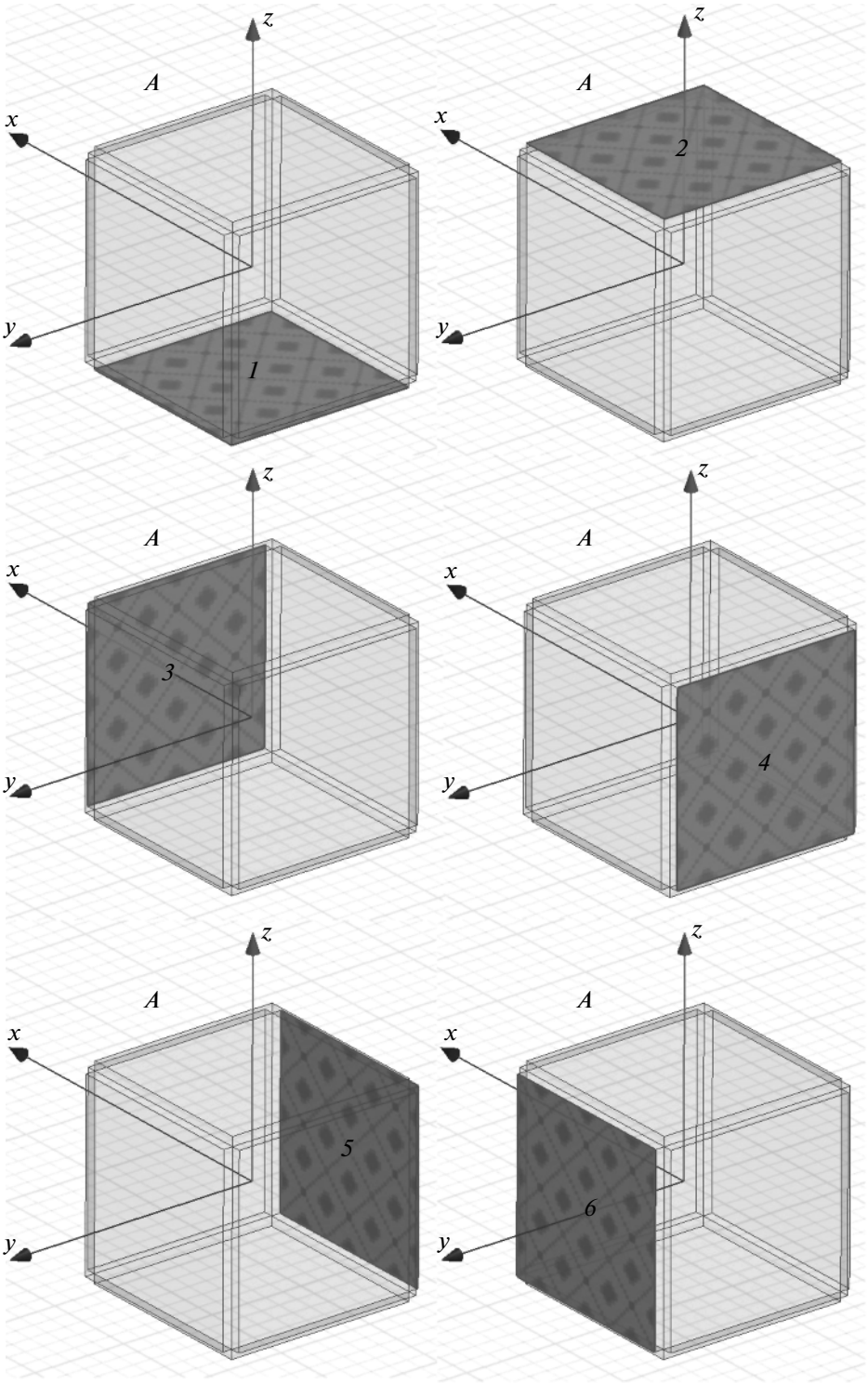

Fig. 4. Faces of rectangular parallelepipeds attached to cube *A*, on which the conditions of excitation and matching of plane waves are imposed.

quency of 150 GHz (half wavelength), the output return loss decreases to −19.32 dB and gradually passes to −30 dB at the frequency of 190 GHz. At the frequency of 300 GHz (the wavelength), the output return loss is −28 dB.

Figure 16 shows the frequency characteristic of the attenuation L as the signal passes from port *2* to port *3* (L_{23}) and from port *2* to port *4* (L_{24}) [13] of the EHSCIE. In the figure we see that at all frequencies, $L_{23} = L_{24}$, which is evident from the symmetry of the

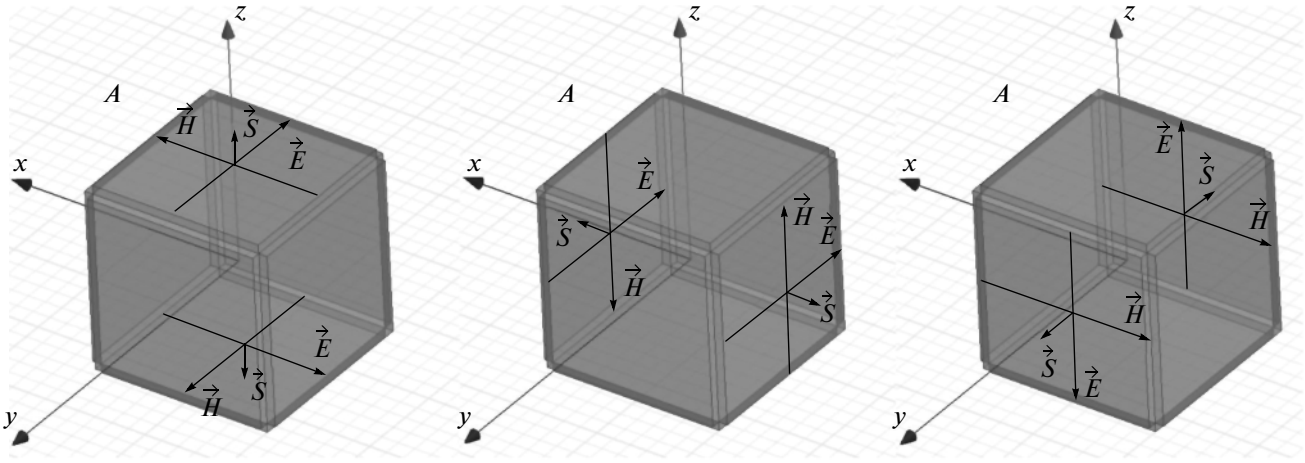

Fig. 5. Direction of the vectors of the electric, $\vec{E}$, and magnetic, $\vec{H}$, fields and the direction of the Poynting vector $\vec{S}$ for the waves incident onto the ports of the external Sestroretskii cube.

geometry. At the frequency of 1 GHz (1/300 of the wavelength), the attenuations L_{23} and L_{24} are −3 dB, i.e., in may be said that the energy incoming to port *2* is divided between ports *3* and *4*. At the frequency of 150 GHz (half wavelength), the attenuations L_{23} and L_{24} take the values of −15.1 dB. At the frequency of 246 GHz, the attenuations L_{23} and L_{24} go on decreasing and take the minimum values −43 dB. Further on, as the frequency increases to 300 GHz, the values of L_{23} and L_{24} increase and reach −35 dB.

Figure 17 shows the frequency characteristic of isolations J between ports *2* and *5* (J_{25}) and between ports *2* and *6* (J_{26}) of the EHSCIE. As is evident from the figure, at all frequencies, the values of the isolations are equal: $J_{25} = J_{26}$. At the frequency of 1 GHz (1/300 of the wavelength), J_{25} and J_{26} are −33.98 dB. As the frequency increases to 55 GHz, the isolations J_{25} and J_{26} increase to −16.87 dB. With a further increase in frequency to 126 GHz, the values of the isolations decrease to −23.20 dB. At the frequency of 150 GHz (the EHSCIE edge length equals to the half-wavelength), we observe a typical resonance the EHSCIE, in which the minimum values of the isolations J_{25} and J_{26} are −28.71 dB. The isolations J_{25} and J_{26} increase to −17.5 dB at the frequency of 180 GHz. Further on, as the frequency increases to 300 GHz, the isolations J_{25} and J_{26} go on decreasing and reach the values of −31.24 dB.

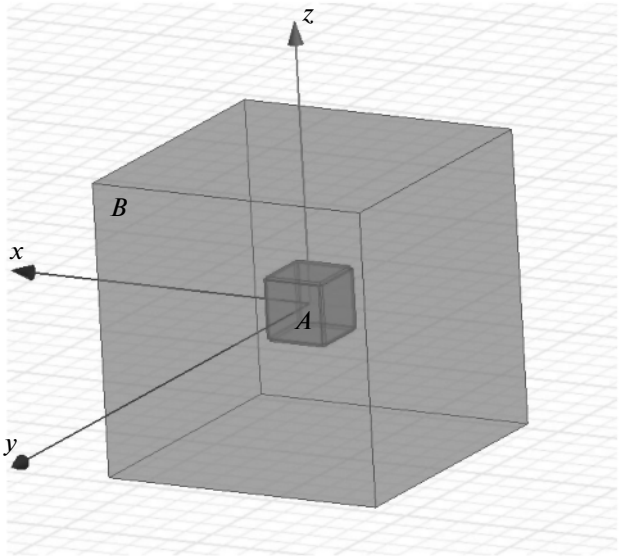

Fig. 6. Geometry of the external electrodynamic problem in the ANSYS HFSS v.15 code.

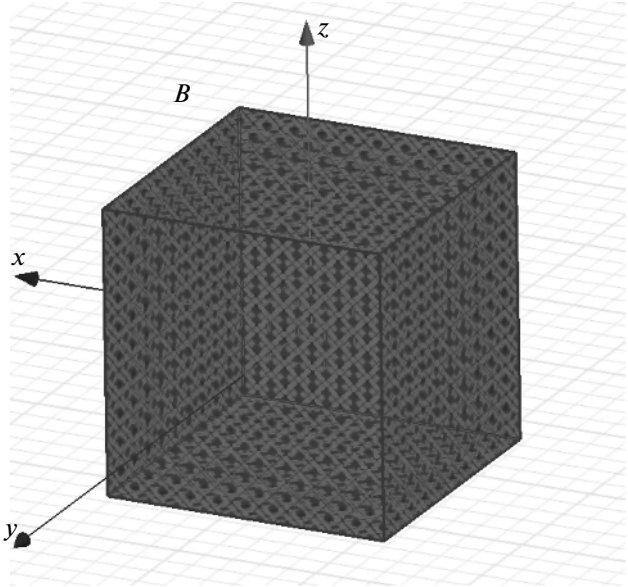

Fig. 7. Radiation boundary conditions on the faces of air cube *B*.

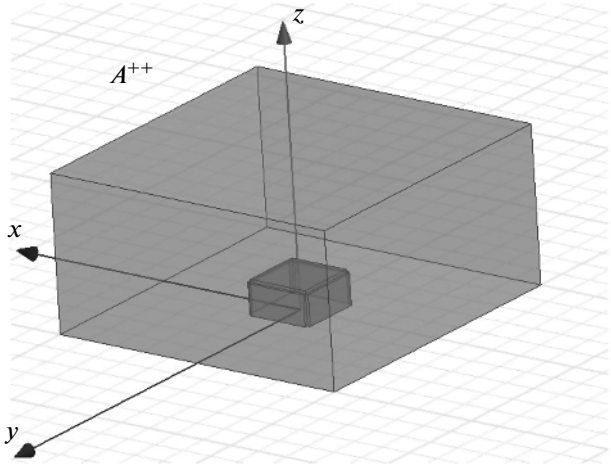

Fig. 8. Geometry of the EHSCIE A^{++}.

The frequency characteristics of the phase φ of the transmission coefficient from port *2* to port *3* $\arg(S_{23})$, and from port *2* to port *4* $\arg(S_{24})$, of the EHSCIE are presented in Fig. 18. Due to the symmetry of the geometry of the EHSCIE, the phases of the signal passing from port *2* to port *3* and from port *2* to port *4* are equal at all frequencies, as is evident from Fig. 18. It should be noted that the phases of the transmission coefficient, $\arg(S_{23})$ and $\arg(S_{24})$, calculated by the ANSYS HFSS v.15 code were divided by π radians [14–16], because the ANSYS HFSS v.15 code chooses the opposite polarization of the electric field for these ports of the EHSCIE. The frequency characteristics of the delay were calculated by the following formulas:

$$\Delta t_{23} = \frac{\arg(S_{23}) - \pi}{2\pi f}, \quad (1)$$

$$\Delta t_{24} = \frac{\arg(S_{24}) - \pi}{2\pi f}, \quad (2)$$

where Δt_{23} is the delay in seconds of the signal passing from port *2* to port *3*, Δt_{24} is the delay of the signal passing from port *2* to port *4*, $\arg(S_{23})$ is the phase of the transmission coefficient from port *2* to port *3* in radians, $\arg(S_{24})$ is the phase of the transmission coefficient from port *2* to port *4*, and *f* is the frequency in hertzs.

Figure 19 shows the frequency characteristic of the delay of the signal passing from port *2* to port *3* (t_{23}) and from port *2* to port *4* (t_{24}) of the EHSCIE. As is evident from Fig. 19, the delay of the signal passing from port *2* is –3.45 ps at the frequency of 1 GHz. With an increase in frequency, the delay decreases in the absolute value. At the frequency of 150 GHz (half the wavelength), the signal delay is –2.97 ps and, at the frequency of 300 GHz (one wavelength), the signal delay is –0.3 ps.

4. THE EXTERNAL SESTRORETSKII CUBE UNDER ANTIPHASE EXCITATION

Now consider the external Sestroretskii cube under the antiphase excitation of ports *1* and *2* (see Fig. 4). Under such an excitation, the problem of electromagnetic-wave scattering is equivalent to the problem with the geometry shown in Fig. 20, which is the upper half of the external Sestroretskii cube (see Fig. 6) on the lower face of which the SC condition is imposed [2, 9–13]. This geometry will be called the geometry of the external half of the Sestroretskii cube under antiphase excitation (EHSCAE) and denoted by A^{+-}.

Figure 21 shown the faces of an EHSCAE on which the OC boundary conditions are imposed, and Fig. 22 shows the faces of an EHSCAE with the SC boundary conditions. The numeration of the ports on which the boundary conditions of matching and excitation of electromagnetic waves are imposed is the same as in the initial geometry (see Fig. 5).

Figure 23 shows the faces of the EHSCAE on which the boundary conditions of excitation and matching of plane waves are imposed [2–4]. The polarizations of the electric, $\vec{E}$, and magnetic, $\vec{H}$, fields and the directions of the Poynting vectors $\vec{S}$ [5–8] of these plane waves are shown in Fig. 24.

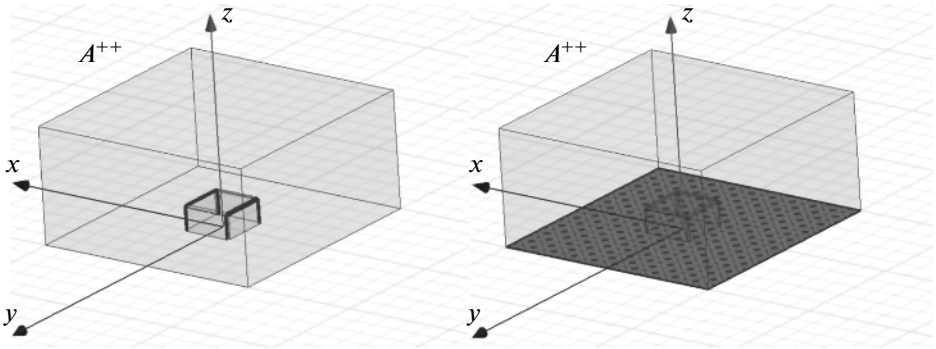

Fig. 9. Geometry of the EHSCIE A^{++} on which the OC condition is imposed.

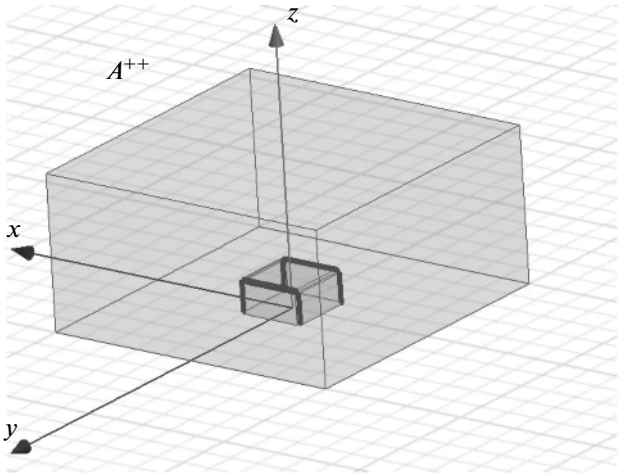

Fig. 10. Geometry of the EHSCIE A^{++} on which the SC condition is imposed.

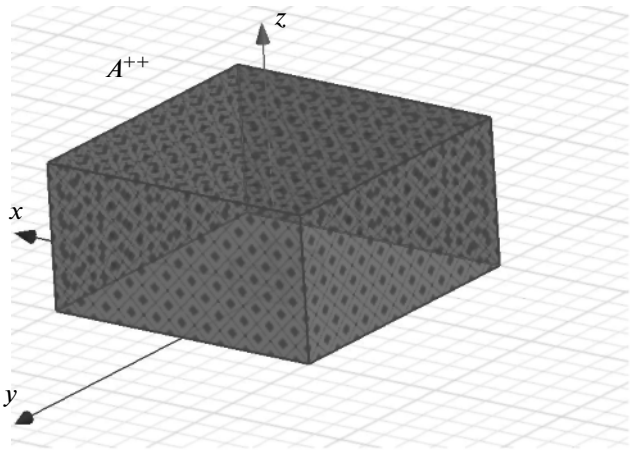

Fig. 11. Radiation boundary conditions for the EHSCIE A^{++}.

The simulation of the problem of electromagnetic-wave scattering by the EHSCAE was performed by means of the ANSYS HFSS v.15 software package for 3D electromagnetic modeling [11].

5. RESULTS OF SIMULATION OF A HALF OF THE SESTRORETSKII CUBE UNDER ANTIPHASE EXCITATION

Since the geometry of the EHSCAE is dual [17] to the geometry of the EHSCIE on the rotations of the EHSCAE about the axis z by 90°, the frequency characteristics of the SWR, isolation, phases of the transmission coefficients, and delay (see Figs. 14–20) will be the same as those for the EHSCIE after the following replacement of the numerations of ports: port *2* of the EHSCIE corresponds to port *2* of the EHSCAE, port *3* of the EHSCIE corresponds to port *5* of the EHSCAE, port *5* of the EHSCIE corresponds to port *4* of the EHSCAE, port *4* of the EHSCIE corresponds to port *6* of the EHSCAE, and port *6* of the EHSCIE corresponds to port *3* of the EHSCAE. Therefore, it is not necessary to perform calculations.

The full scattering matrix of the external Sestroretskii cube is found from the scattering matrices of the EHSCIE and EHSCAE by the method presented in [2, 9–12].

6. RESULTS OF SIMULATION OF THE EXTERNAL SESTRORETSKII CUBE

The scattering matrix of the external Sestroretskii cube is determined from the scattering matrices of the EHSCIE and EHSCAE by the method presented in [2, 9–12], taking into account that under the in-phase and antiphase excitations ports *3*, *4*, *5*, and *6* of the Sestroretskii cube are divided in two halves. Let us present calculated frequency characteristics of the external Sestroretskii cube, starting from the frequency characteristics of the EHSCIE and EHSCAE.

The plots of the frequency characteristics of the SWR and the absolute value of the reflection coefficient for port *2* of the external Sestroretskii cube coincide with the corresponding plots for the EHSCIE (see Figs. 14, 15).

Figure 25 shows the frequency characteristics of the transmission coefficient from port *2* to ports *3–6* of the external Sestroretskii cube. For comparison, the frequency characteristics of the transmission coefficient from port *2* to ports *3* and *4* of the EHSCIE are also presented. As we see from the figure, the plots of the transmission coefficient from port *2* to ports *3, 4, 5*, and *6* coincide. This is evident from the symmetry. At the frequency of 1 GHz (the edge length of the external Sestroretskii cube is 1/300 of the wavelength), the coefficient is −6.19 dB. Up to the frequency of 120 GHz (2/5 of the wavelength), the transmission coefficient decreases to −14.12 dB. At the frequency of 150 GHz (the edge length of the external Sestroretskii cube is half the wavelength), we see a typical resonance of the frequency characteristics of the external Sestroretskii cube and the transmission coefficient is −16.81 dB. Further on, the transmission coefficient of the external Sestroretskii cube goes on decreasing and, at the frequency of 294 GHz, equals −34.72 dB. At the frequency of 300 GHz, the transmission coefficient of the external Sestroretskii cube is −32 dB.

As we see, up to half the wavelength, until the initiation of higher modes, the behavior of the transmission coefficient of the external Sestroretskii cube corresponds to the behavior of the transmission coefficient of the EHSCIE and their values differ by 3 dB. This is clear, because, in the EHSCIE, the energy supplied to port *2* is divided among two ports: *3* and *4* and, in the full external Sestroretskii cube, the energy supplied to port *2* is divided among four ports: *3, 4, 5*, and *6*. Up to the frequency of 120 GHz, the isolation between

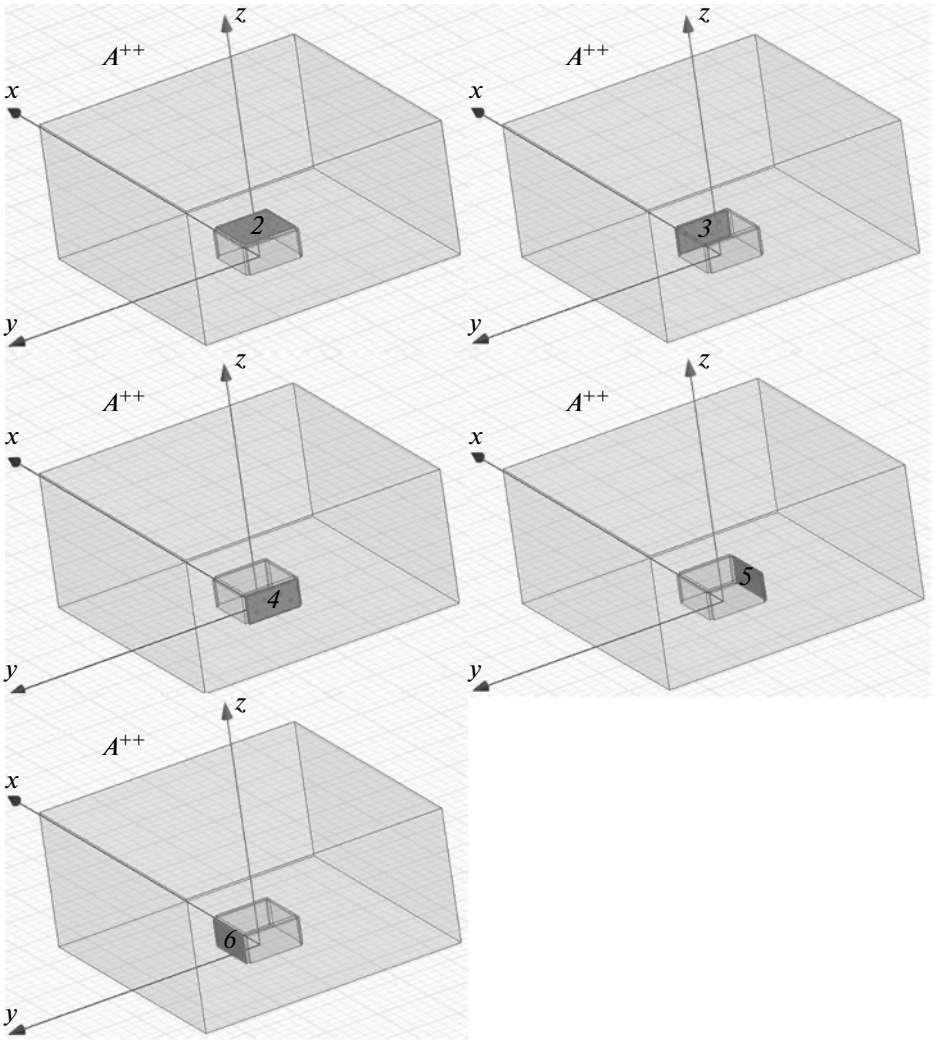

Fig. 12. Faces of the EHSCIE A^{++}, on which the conditions of excitation and matching of plane waves are imposed.

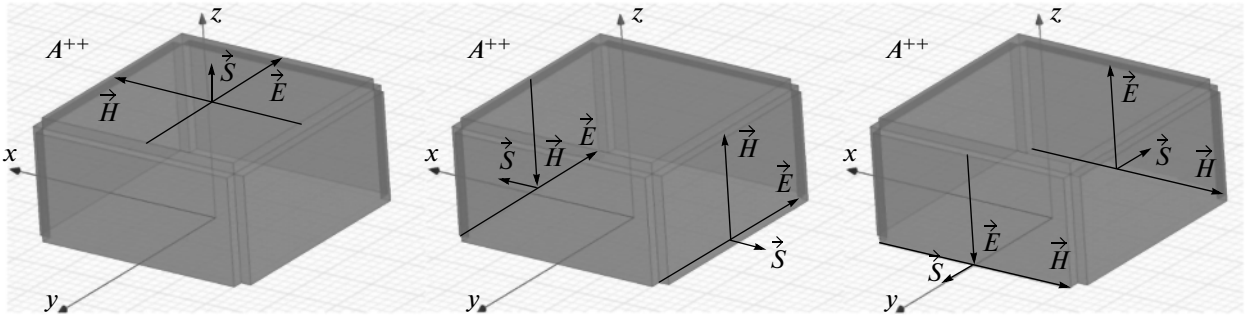

Fig. 13. Direction of the vectors of the electric, $\vec{E}$, and magnetic, $\vec{H}$, fields and the direction of the Poynting vectors $\vec{S}$ for the waves incident onto the ports of the EHSCIE A^{++}.

ports *2*, *5*, and *6* of the EHSCIE is below –25 dB (see Fig. 17). At the frequency above 120 GHz, the isolation decreases and, above 150 GHz, waveguide modes become propagating. As a result, the behavior of the transmission coefficient of the external Sestroretskii cube is different from that of the EHSCIE.

The frequency characteristic of the phase of the transmission coefficient from port *2* to ports *3*, *4*, *5*, and *6* of the external Sestroretskii cube is presented in Fig. 26. For comparison, the frequency characteristic of the phase of the transmission coefficient from port *2* to ports *3* and *4* of the EHSCIE is presented. Due to

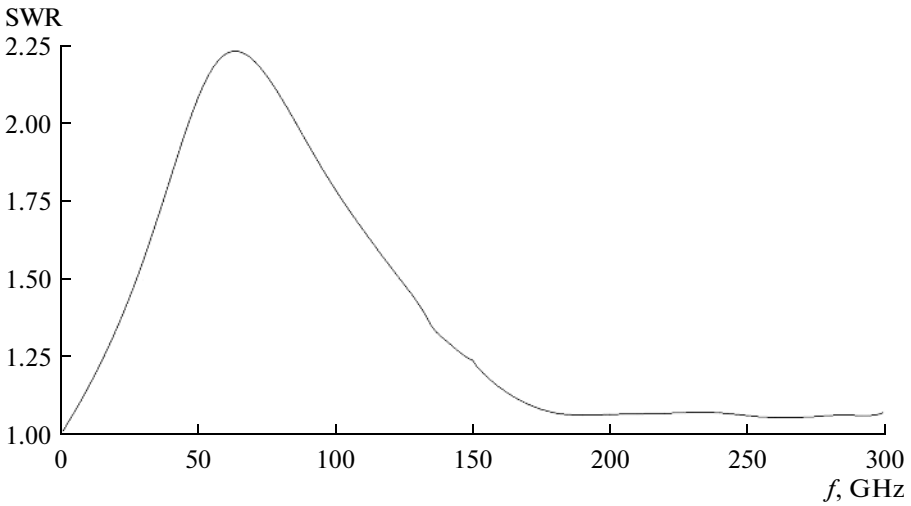

Fig. 14. Frequency characteristic of the SWR of the EHSCIE for port *2*, calculated by the ANSYS HFSS v.15 code.

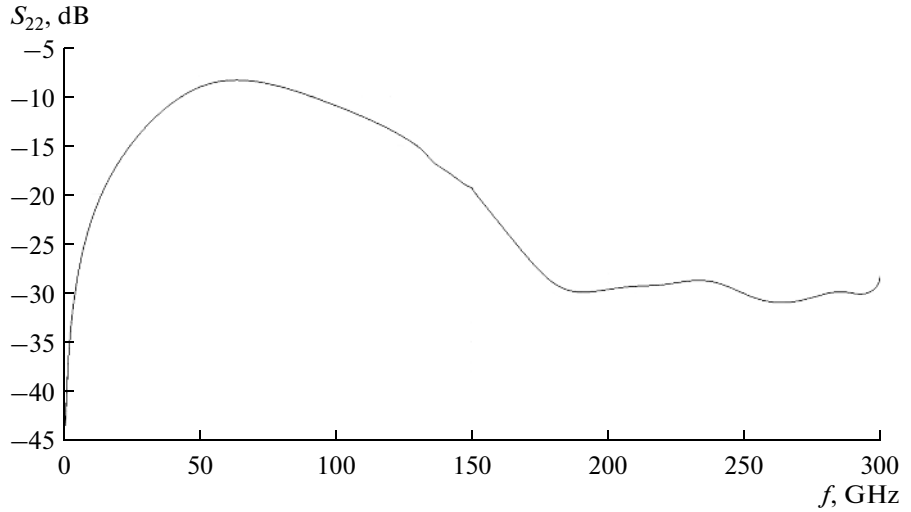

Fig. 15. Frequency characteristic of the reflection coefficient of the EHSCIE for port *2*, calculated by the ANSYS HFSS v.15 code.

the symmetry of the geometry of the external Sestroretskii cube, the phases of the transmission coefficient from port *2* to ports *3*, *4*, *5*, and *6* are equal at all frequencies, which is evident from Fig. 26.

As we see, up to the frequency of 120 GHz (the edge length of the external Sestroretskii cube is 2/5 of the wavelength), the phase of the transmission coefficient of the external Sestroretskii cube equals the phase of the transmission coefficient of the EHSCIE. In contrast to the absolute value of the transmission coefficient, the phase of the transmission coefficient depends on the isolation more strongly. The phases of the transmission coefficient of the EHSCIE and the external Sestroretskii cube have practically the same behavior, linearly decreasing practically from zero at the frequency of 1 GHz to –133° at the frequency of 120 GHz. Then, after the frequency of 150 GHz (the edge length of the external Sestroretskii is half the wavelength), substantial distinctions are observed.

Figure 27 shows the frequency characteristic of the delay of the signal from port *2* to ports *3*, *4*, *5*, and *6* of the external Sestroretskii cube. For comparison, the frequency characteristic of the delay of the signal from port *2* to ports *3* and *4* of the EHSCIE are presented. As is evident from the figure, the delay for ports *3*, *4, 5*, and *6* is –2.84 ps at the frequency of 1 GHz. At the frequencies of 150 GHz (the edge length of the external Sestroretskii is half the wavelength) and 250 GHz, we observe typical resonances in the delay.

From Fig. 27 we see that the frequency characteristic of the delay of the external Sestroretskii cube and the EHSCIE are substantially different. Apparently, it is connected with a significant isolation between ports *2* and *5, 6* of the EHSCIE (see Fig. 17). The isolation becomes less than –25 dB already

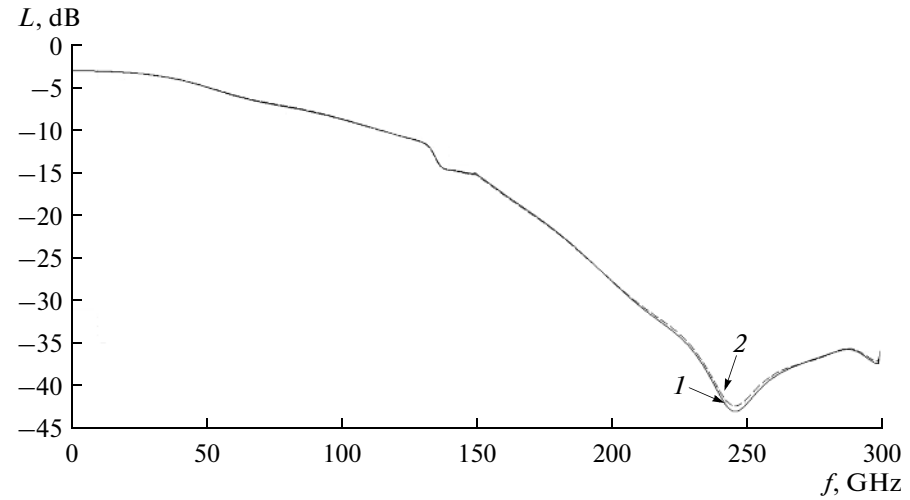

Fig. 16. Frequency characteristics of the attenuation of the signal passing from port *2* to port *3* (L_{23}) and from port *2* to port *4* (L_{24}) for the EHSCIE, calculated by the ANSYS HFSS v.15 code: (curve *1*) port *3*, (curve *2*) port *4*.

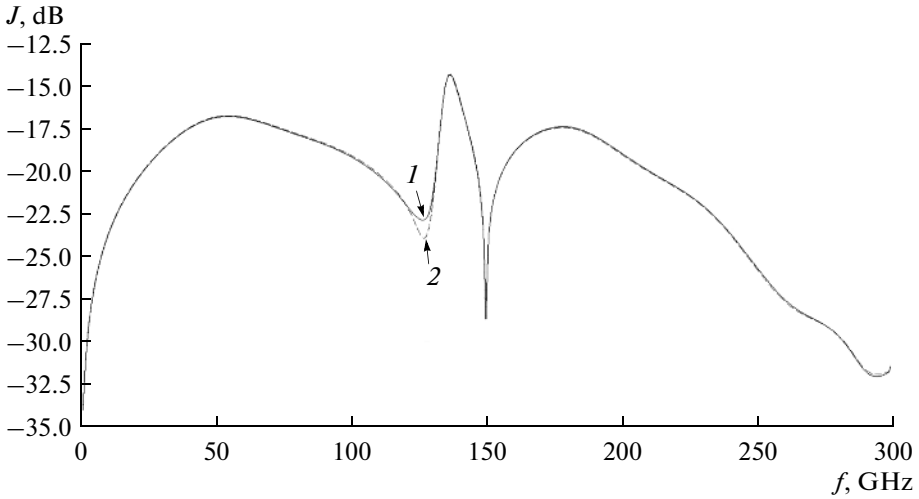

Fig. 17. Frequency characteristics of the isolations J_{25} and J_{26} of the EHSCIE, calculated by the ANSYS HFSS v.15 code: (curve *1*) port *5*, (curve *2*) port *6*.

above the frequency of 10 GHz and then decreases to –17 dB at the frequency of 50 GHz; further on, it increases again to –22.5 dB at the frequency of 125 GHz. Such a frequency behavior of the isolation leads to a significant difference in the frequency dependence of the delay for the full external Sestroretskii cube, because the delay is a derivative of the phase of the transmitted signal. Such a small isolation is caused by the fact that the ports of the external Sestroretskii cube have the length $h = 0.05$ mm (see Fig. 1).

It is of interest to consider the frequency characteristic of the power P_{rad} radiated to the external space, which can be calculated by the following relationship:

$$P_{\text{rad}}(\text{dB}) = 10\log(1 - (|S_{21}|^2 + |S_{22}|^2 + |S_{23}|^2 + |S_{24}|^2 + |S_{25}|^2 + |S_{26}|^2)), \quad (3)$$

where $|S_{21}|^2$, $|S_{22}|^2$, $|S_{23}|^2$, $|S_{24}|^2$, $|S_{25}|^2$, and $|S_{26}|^2$ are the squared absolute values of scattering matrix of the external Sestroretskii cube, calculated by the ANSYS HFSS v.15 code.

The power P_{nrad} not radiated to the external space is the sum of the energies of reflected waves at ports *1*, *2*, *3*, *4*, *5*, and *6* of the external Sestroretskii cube when energy is fed to port *2*:

$$P_{\text{nrad}}(\text{dB}) = 10\log(|S_{21}|^2 + |S_{22}|^2 + |S_{23}|^2 + |S_{24}|^2 + |S_{25}|^2 + |S_{26}|^2). \quad (4)$$

Figure 28 presents the plotted frequency dependences of the powers P_{rad} and P_{nrad} for the external Sestroretskii cube (curves *1*, *2*) and the external Huygens cubes (curves *3*, *4*) [14–16]. As is evident from Fig. 28, up to the frequency of 17 GHz, the P_{rad} for the external Sestroretskii cube (curve *1*) is undefined,

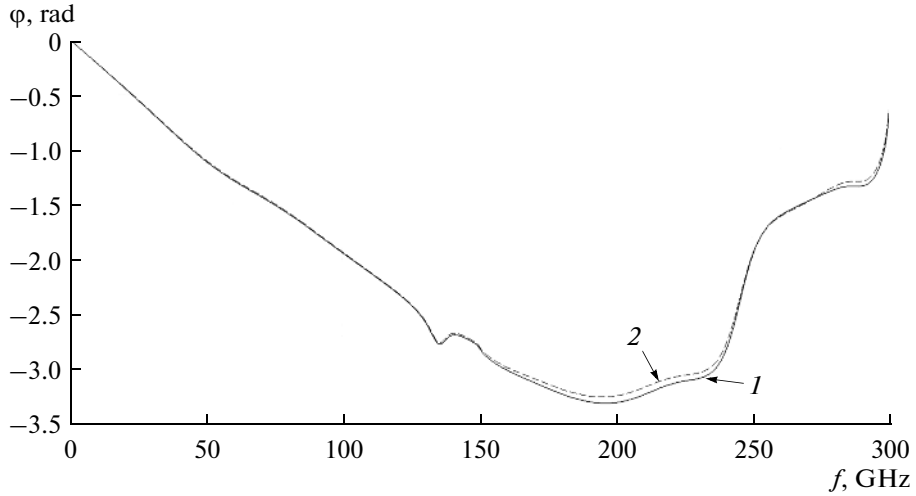

Fig. 18. Frequency characteristics of the phase of the transmission coefficient from port *2* to port *3* $\arg(S_{23})$, (curve *1*) and from port *2* to port *4* $\arg(S_{24})$, (curve *2*) for the EHSCIE, calculated by the ANSYS HFSS v.15 code.

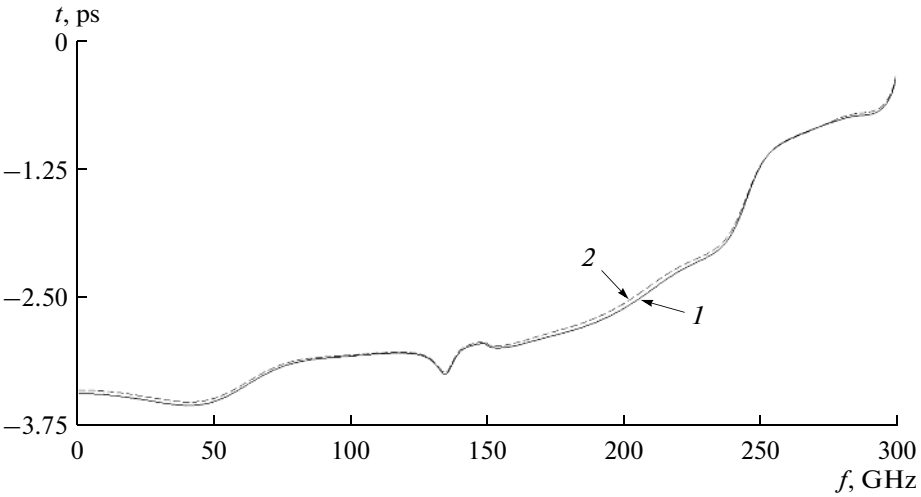

Fig. 19. Frequency characteristics of the delay of the signal passing from port *2* to port *3*, (curve *1*) and from port *2* to port *4*, (curve *2*) of the EHSCIE, calculated by the ANSYS HFSS v.15 code.

because it is below zero. This is connected with the inaccuracy of calculations by the ANSYS HFSS v.15 code [4]. Starting from the frequency of 17 GHz, the P_{rad} for the external Sestroretskii cube increases from −30.4 dB to −3 dB at the frequency of 66 GHz. At the frequency of 113.5 GHz, the frequency characteristics of the P_{rad} for the external Sestroretskii cube (curve *1*) and the external Huygens cube (curve *3*) intersect one another at the value of −1.09 dB. Further on, up to the frequency of 300 GHz, the frequency characteristics of the P_{rad} for the external Sestroretskii cube tends to 0 dB.

As is evident from Fig. 28, the energy loss by radiation for the external Sestroretskii cube is greater than that for the external Huygens cube up to the frequency of 113.5 GHz. However, at the frequency above 113.5 GHz, the energy loss by radiation for the external Sestroretskii cube is only a little lower than that for the external Huygens cube. At low frequencies, practically all power P_{nrad} (see Fig. 28) returns to the external Sestroretskii cube (curve *2*). With an increase in frequency, the returned energy decreases. At the frequency of 66 GHz, the power P_{nrad} returned to the external Sestroretskii cube equals the power P_{rad} radiated to the external space. It should be noted that, at the frequency of 58.3 GHz, for the external Huygens cube, the frequency dependences of the radiated power P_{rad} and returned power P_{nrad} intersect one another.

Figure 29 shows the theoretical (curve *1*) and simulated (curve *2*) frequency characteristics of the gain factor of the external Sestroretskii cube.

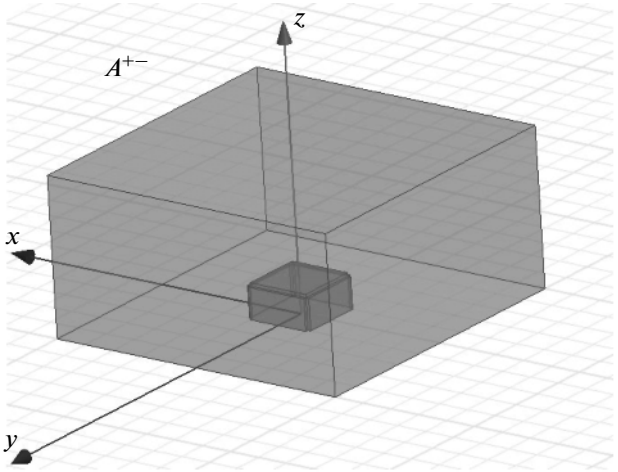

Fig. 20. Geometry of the EHSCAE A^{+-}.

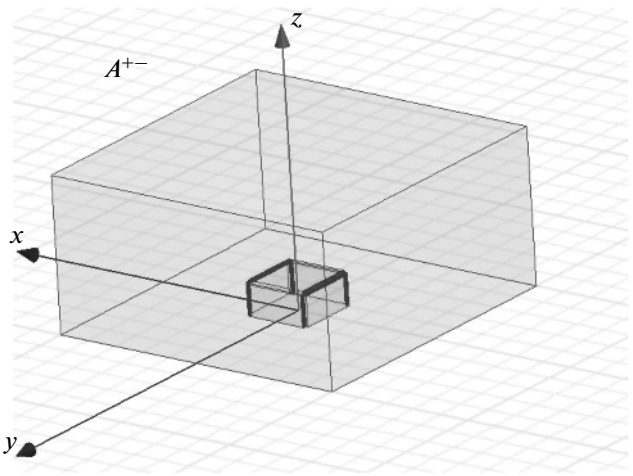

Fig. 21. Geometry of the EHSCAE A^{+-} on which the OC condition is imposed.

As the theoretical limit for the frequency dependence of the gain factor, we take the following relationships [14–16]:

$$K_{\text{gain}}\,(\text{dB}) = k + 20\log f', \qquad (5)$$

where $k = 10\log\left(\frac{4\pi}{9}\times 10^{-4}\right) = -38.55$ dB $= K_{\text{gain}}$ (dB) at $f' = 1$ GHz.

The dependence corresponding to expression (5) for K_{gain} is illustrated by curve *1* in Fig. 29.

Consider the simulated (curve *2*) frequency characteristics of the gain factor for the external Sestroretskii cube. Starting from the frequency of 1 GHz (1/300 of the wavelength), K_{gain} increases from –67.26 dB to –27.29 dB at the frequency of 10 GHz (1/30 of the wavelength). With a further increase in the frequency, K_{gain} increases to –15.31 dB at 20 GHz. At the frequency of 55 GHz, $K_{\text{gain}} = 0.03$ dB. With a further increase in frequency, K_{gain} increases to 3.1 dB at the frequency of 85 GHz and to 8.9 dB at the frequency of 210 GHz. Then K_{gain} gradually increases to 11.82 dB at the frequency of 300 GHz (one wavelength).

7. COMPARISON OF THE SCATTERING MATRICES OF THE INTERNAL AND EXTERNAL SESTRORETSKII CUBES

The external and internal [14] Sestroretskii cubes are 12-terminal devices. Let us compare their scattering matrices for the quasi-static cases, i.e., at the frequencies tending to zero. For numerical calculations, the comparison was made at the frequency of 1 GHz. The results are presented in the table.

The analysis of the table leads to the following conclusion: in the quasi-static case, the external and internal Sestroretskii cubes are similar in the sense that they are matched and almost all energy is transmitted from port *2* to ports *3*, *4*, *5*, and *6*. They differ in the phases of the transmission coefficients (phases S_{23}, S_{24}, S_{25}, S_{26}), i.e., in the delays of the signal passing from port *2* to ports *3*, *4*, *5*, and *6*. In the quasi-static

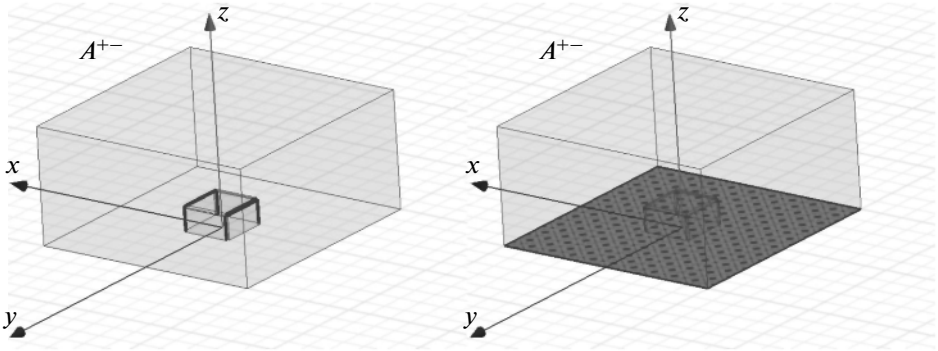

Fig. 22. Geometry of the EHSCAE A^{+-} on which the SC condition is imposed.

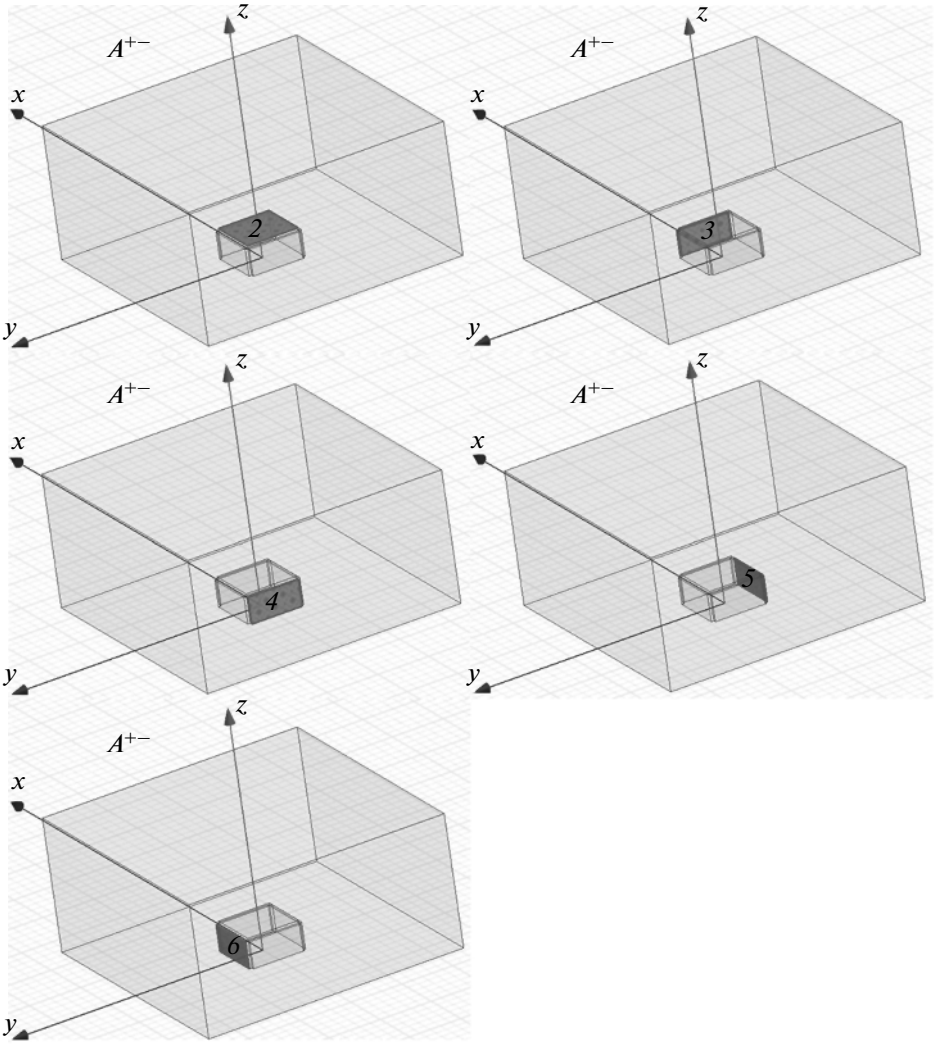

Fig. 23. Faces of the EHSCAE A^{+-}, on which the conditions of excitation and matching of plane waves are imposed.

case, the external Sestroretskii cube practically does not radiate energy and almost all energy is transmitted to ports *3*, *4*, *5*, and *6*.

Comparison of the absolute values and phases of the scattering matrices of the internal and external Sestroretskii cubes

Frequency characteristics	Values or the internal Sestroretskii cube at the frequency of 1 GHz	Values for the external Sestroretskii cube at the frequency of 1 GHz
$\|S_{22}\|$, dB	−74.48	−43.15
Phase S_{22}, rad	−1.55	−1.59
$\|S_{23}\|$, $\|S_{24}\|$, dB	−6.02	−6.02
Phase S_{23}, S_{24} rad	−0.01	−0.02
$\|S_{25}\|$, $\|S_{26}\|$, dB	−36.06	−33.98
Phase S_{25}, S_{26}, rad	−2.35	−2.38
Delay, ps	1.65	3.45

8. THE EXTERNAL SESTRORETSKII CUBE AS A DIPLEXER AND QUADRUPLEXER

1. For the frequencies of 1 to 16 GHz and of 150 to 300 GHz, the SWR of port *2* does not exceed 1.25 (see Fig. 14). At the frequencies of 16 to 150 GHz, the SWR does not exceed 2.25. The corresponding frequency dependence of the reflection coefficient is shown in Fig. 15, from which we see that the absolute value of the reflection coefficient does not exceed −20 dB at the frequencies below 14.4 GHz and above 151.67 GHz.

2. The frequency dependences of the transmission coefficient from port *2* to ports *3*, *4*, *5*, and *6* (phases L_{23}, L_{24}, L_{25}, L_{26}) for the external Sestroretskii cube are as follows (see Fig. 25):

at the frequency of 1 GHz, L_{23}, L_{24}, L_{25}, and L_{26} equal −6.02 dB;

with an increase in frequency, L_{23}, L_{24}, L_{25}, and L_{26} monotonically decrease to −14 dB at the frequency of 120 GHz;

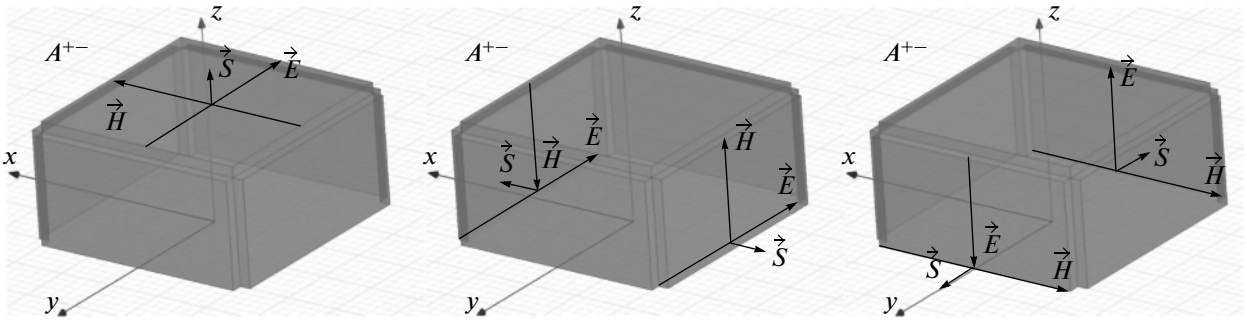

Fig. 24. Direction of the vectors of the electric, $\vec{E}$, and magnetic, $\vec{H}$, fields and the direction of the Poynting vectors $\vec{S}$ for the waves incident onto the ports of the EHSCAE A^{+-}.

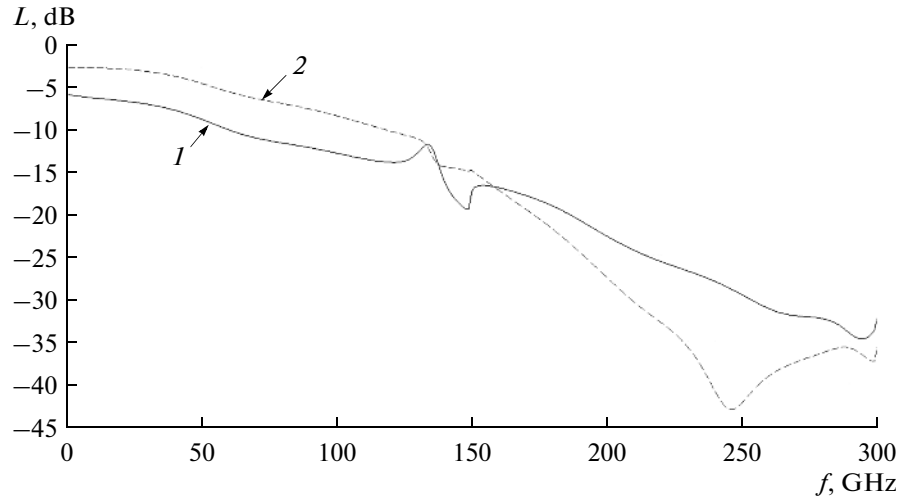

Fig. 25. Frequency characteristic of the transmission coefficient from port *2*: (curve *1*) to ports *3*, *4*, *5*, and *6* (the external Sestroretskii cube) and (curve *2*) to ports *3* and *4* (EHSCIE).

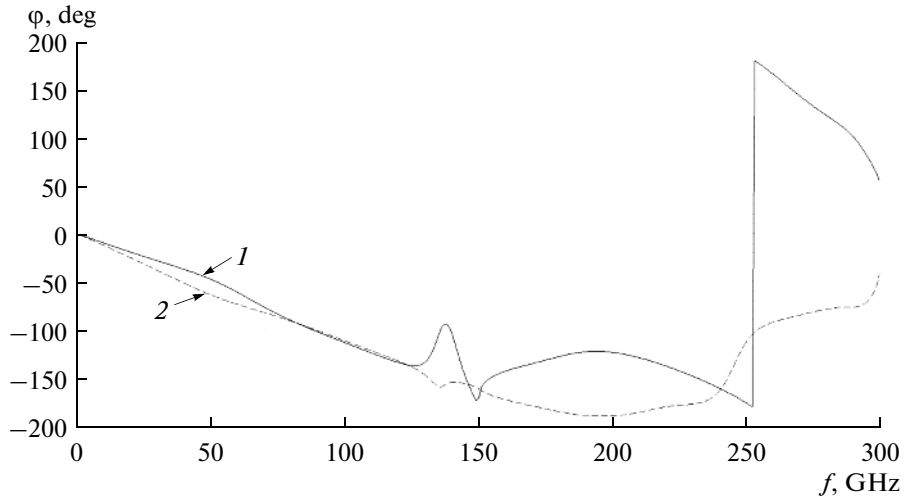

Fig. 26. Frequency characteristic of the phase of the transmission coefficient from port *2*: (curve *1*) to ports *3*, *4*, *5*, and *6* (the external Sestroretskii cube) and (curve *2*) to ports *3* and *4* (EHSCIE).

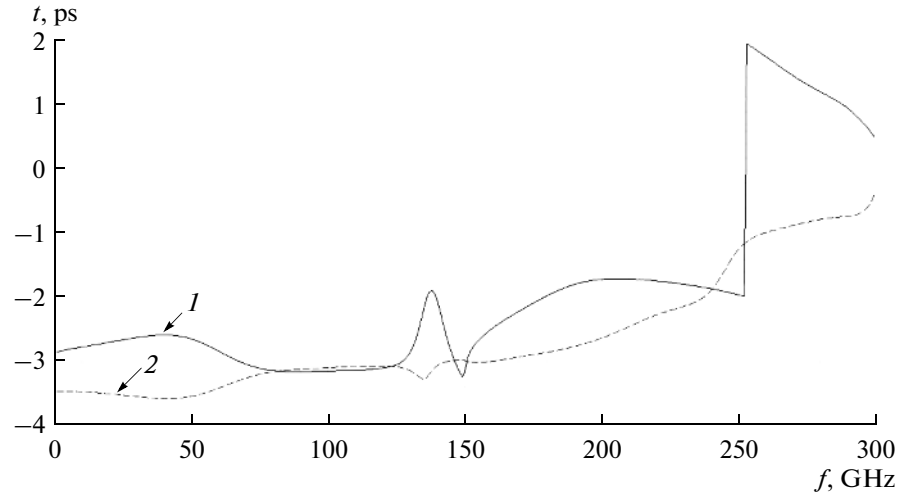

Fig. 27. Frequency characteristic of the phase of the delay of the signal passing from port *2*: (curve *1*) to ports *3*, *4*, *5*, and *6* (the external Sestroretskii cube) and (curve *2*) to ports *3* and *4* (EHSCIE).

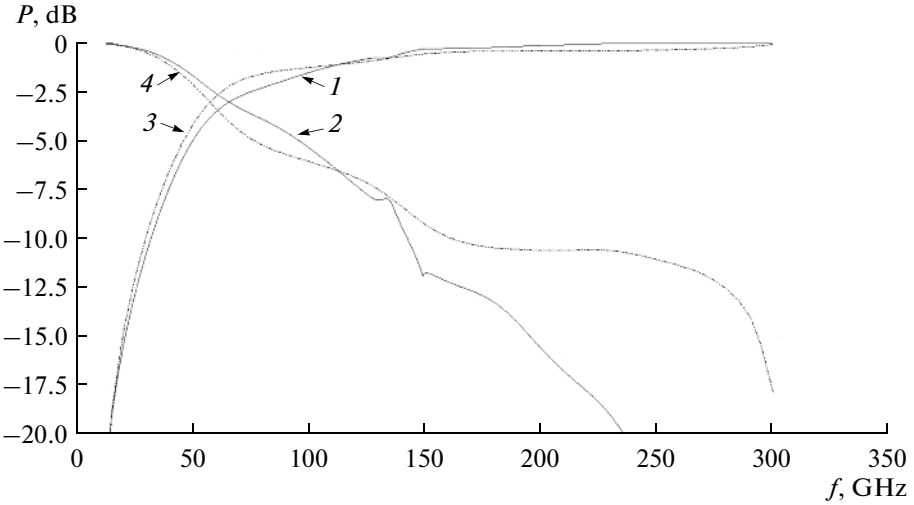

Fig. 28. Comparison of the frequency characteristic of the radiated, P_{rad}, and not radiated power, P_{nrad} for (curves *1*, *2*) the external Sestroretskii cube and (curves *3*, *4*) the Huygens cube.

in the region of 150 GHz, L_{23}, L_{24}, L_{25}, and L_{26} have a resonance character;

from the frequency of 155 GHz, L_{23}, L_{24}, L_{25}, and L_{26} monotonically decrease to −34.7 dB at the frequency of 290 GHz;

in the region of 300 GHz, the frequency dependence of the transmission coefficient also has a resonance character.

3. The frequency dependences of the power P_{rad} radiated to the free space is as follows (see Fig. 28):

at the frequency below 42 GHz, the power P_{rad} is below −3 dB;

at the frequency above 42 GHz, the power P_{rad} is above −3 dB.

The simultaneous fulfillment of conditions 1–3 makes it possible to consider the external Sestroretskii cube a frequency diplexer and quadruplexer [18–20].

The analysis of the frequency characteristics presented above leads to the following conclusion.

1. The above-considered external Sestroretskii cube is described sufficiently well in the single-mode approximation and has the properties of a waveguide triplexer [2] up to the frequencies of 16 GHz (the edge length of the external Sestroretskii cube is of 4/75 of the wavelength):

(a) port *2* is matched and isolated from ports *3*, *4*, *5*, and *6*;

(b) all energy incoming to port *2* is divided in equal proportions among ports *3*, *4*, *5*, and *6*;

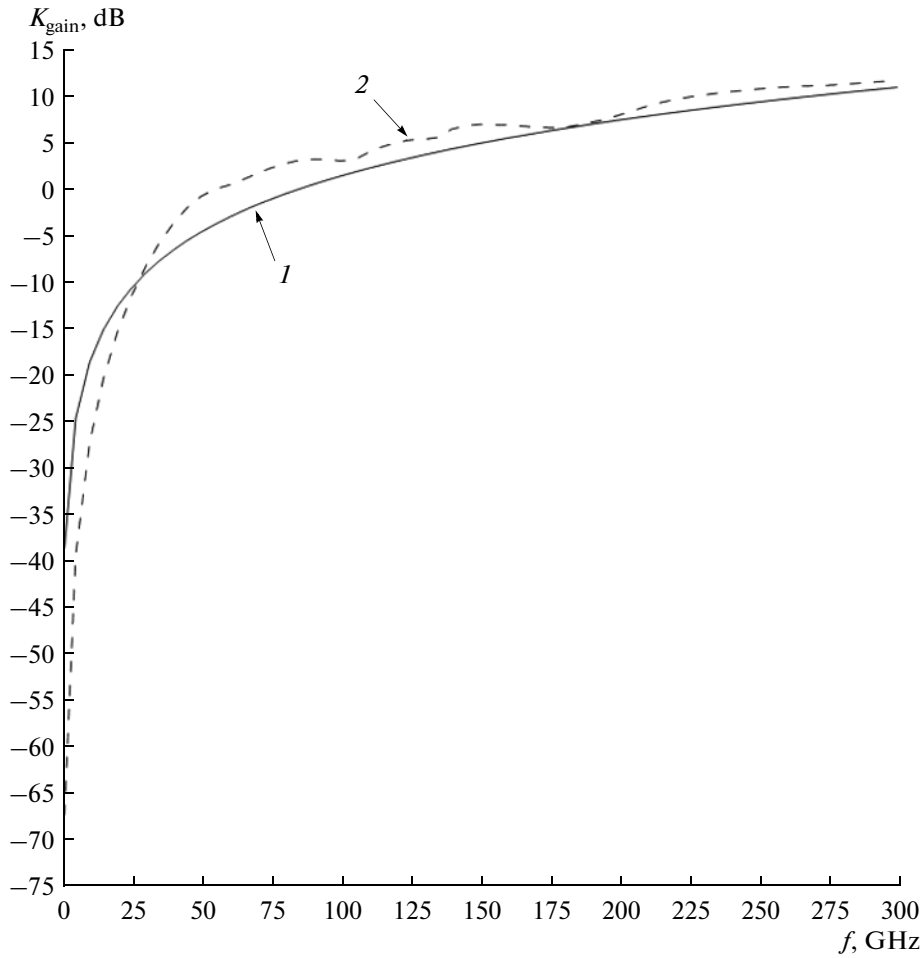

Fig. 29. (Curve *1*) Theoretical and (curve *2*) simulated with the use of the ANSYS HFSS v. 15 code frequency characteristics of the gain factor for the external Sestroretskii cube.

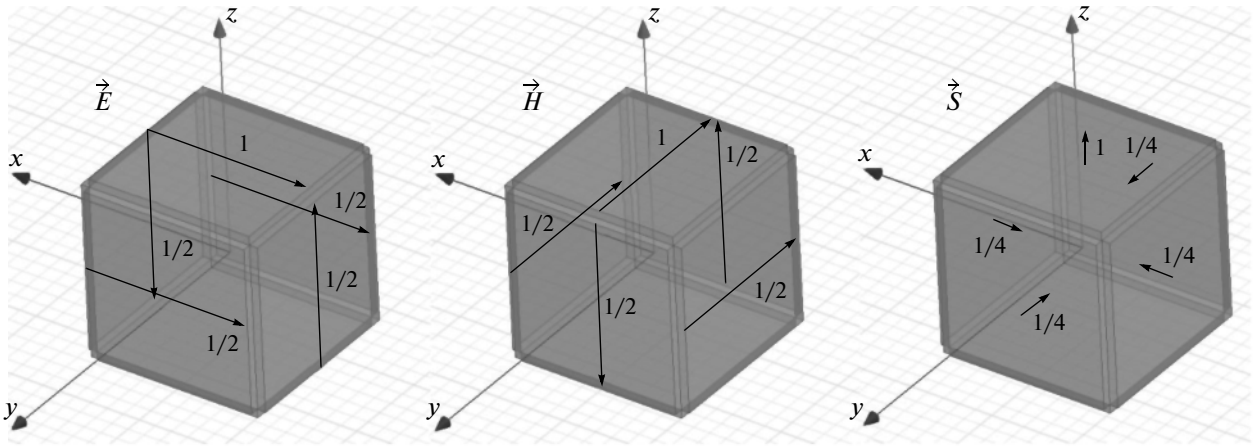

Fig. 30. Directions of the vectors of the electric, $\vec{E}$, and magnetic, $\vec{H}$, fields and the direction of the Poynting vectors $\vec{S}$ for the wave incident onto port *2* and waves transmitted to ports *3*, *4*, *5*, and *6* of the external Sestroretskii cube.

(c) if the amplitude of the electric and magnetic fields of the incident waves to port *2* is taken as unity, then the amplitudes of the wave incident to ports *3*, *4*, *5*, and *6* are 1/2;

(d) if the amplitude of the power flux density of the waves incident to port *2* is taken as unity, then the amplitudes of the wave incident to ports *3*, *4*, *5*, and *6* are 1/4;

(e) the directions of the vectors $\vec{E}$ and $\vec{H}$ of the electric and magnetic fields and the vectors of the energy flux densities of the waves incident to port *2* and transmitted to ports *3*, *4*, *5*, and *6* of the external Sestroretskii cube are shown in Fig. 30.

2. The fraction of the radiated energy tends to unity as the edge length of the external Sestroretskii cube tends to the wavelength; in this case, K_{gain} tends to 11.82 dB.

3. For the external Sestroretskii cube (with the edge length greater than 11/50 of the wavelength), the free space is a sort of a below-cutoff waveguide and the energy loss by radiation exceeds –3 dB.

4. The gain factor of the external Sestroretskii cube becomes positive when the edge length of the external Sestroretskii cube becomes smaller than 11/60 of the wavelength.

5. The external Sestroretskii cube may be considered as a frequency diplexer and quadruplexer.

CONCLUSIONS

Numerical modeling of the external Sestroretskii cube has been performed by means of the ANSYS HFSS v.15 code for electrodynamic simulation. It has been shown that the external Sestroretskii cube has the properties of a double waveguide triplexer for wavelengths greater that 4/75 of the edge length of the external Sestroretskii cube. The external Sestroretskii cube has the properties of a frequency diplexer and quadruplexer.

REFERENCES

1. S. E. Bankov, E. M. Guttsait, and A. A. Kurushin, *Computation of Optical and Microwave Problems by Means of HFSS* (Orkada, Moscow, 2012) [in Russian]. http://jre.cplire.ru/win/library/7/text.pdf.
2. D. M. Sazonov, A. N. Gridin, and B. A. Mishustin, *Microwave Circuits* (Vysshaya Shkola, Moscow, 1981; Mir, Moscow, 1982).
3. K. N. Klimov, D. S. Gezha, and D. O. Firsov-Shibaev, *Practical Application of Electrodynamic Modeling* (Lambert Academic Publishing, Saarbrücken, 2012) [in Russian].
4. K. N. Klimov, D. O. Firsov-Shibaev, and D. S. Gezha, *Method of Impedance Analysis of Electromagnetic Space* (Lambert Academic Publishing, Saarbrücken, 2013) [in Russian].
5. G. T. Markov and D. M. Sazonov, *Antennas* (Energiya, Moscow, 1975) [in Russian].
6. S. I. Baskakov, *Fundamentals of Electrodynamics* (Sovetskoe Radio, Moscow, 1973) [in Russian].
7. M. A. Zheksenov and A. S. Petrov, J. Commun. Technol. Electron. **59**, 289 (2014).
8. M. A. Zheksenov and A. S. Petrov, J. Commun. Technol. Electron. **59**, 427 (2014).
9. B. V. Sestroretskii and Yu. K. Vladimirov, *Computer-Aided Design of Microwave Devices and Systems* (O-vo "Znanie" UkrSSR, Kiev, 1974), Part 1 [in Russian].
10. B. V. Sestroretskii, Vopr. Radioelektron., Ser. Obshchetekhn., No. 2, 113 (1976).
11. B. V. Sestroretskii, in *Interuniversity Collection of Scientific Works. Computer-Aided Design of Microwave Devices and Systems* (MIREA, Moscow, 1977), p. 127 [in Russian].
12. B. V. Sestroretskii, Vopr. Radioelektron., Ser. Obshchie Vopr. Radioelektron., No. 5, 56 (1983).
13. P. B. Johns, IEEE Trans. Microwave Theory Tech. **35**, 370 (1987).
14. A. S. Godin, A. B. Tsai, and K. N. Klimov, J. Commun. Technol. Electron. **60**, 329 (2015).
15. A. S. Godin, A. B. Tsai, and K. N. Klimov, J. Commun. Technol. Electron. **60**, 436 (2015).
16. A. S. Godin, A. B. Tsai, and K. N. Klimov, J. Commun. Technol. Electron. **60**, 737 (2015).
17. N. N. Fedorov, *Fundamentals of Electrodynamics* (Vysshaya Shkola, Moscow, 1980) [in Russian].
18. O. V. Alekseev, G. A. Groshev, and G. G. Chavka, *Multichannel Frequency Dividers and Their Application* (Radio i Svyaz', Moscow, 1981) [in Russian].
19. A. L. Fel'dshtein and L. R. Yavich, *Synthesis of Microwave Two-Port and Four-Port Networks* (Radio i Svyaz', Moscow, 1971) [in Russian].
20. J. L. Altman, *Microwave Circuits* (D. Van Nostrand, New York, 1964; Mir, Moscow, 1968).

Translated by E. Chernokozhin